


Electronuclear Transition into a Spatially Modulated Magnetic State in YbRh₂Si₂

J. Knapp^{Ⓧ,*}, L. V. Levitin^{Ⓧ,†}, J. Nyéki[Ⓧ], A. F. Ho[Ⓧ], B. Cowan, and J. Saunders[‡]
Department of Physics, Royal Holloway University of London, TW20 0EX, Egham, United Kingdom

M. Brando and C. Geibel[Ⓧ]
Max Planck Institute for Chemical Physics of Solids, Nöthnitzer Straße 40, 01187 Dresden, Germany

K. Kliemt[Ⓧ] and C. Krellner[Ⓧ]
Physikalisches Institut, Max-von-Laue-Straße 1, 60438 Frankfurt am Main, Germany

 (Received 6 October 2022; accepted 3 February 2023; published 23 March 2023; corrected 1 October 2024)

The nature of the antiferromagnetic order in the heavy fermion metal YbRh₂Si₂, its quantum criticality, and superconductivity, which appears at low mK temperatures, remain open questions. We report measurements of the heat capacity over the wide temperature range 180 μ K–80 mK, using current sensing noise thermometry. In zero magnetic field we observe a remarkably sharp heat capacity anomaly at 1.5 mK, which we identify as an electronuclear transition into a state with spatially modulated electronic magnetic order of maximum amplitude $0.1 \mu_B$. We also report results of measurements in magnetic fields in the range 0 to 70 mT, applied perpendicular to the c axis, which show eventual suppression of this order. These results demonstrate a coexistence of a large moment antiferromagnet with putative superconductivity.

DOI: [10.1103/PhysRevLett.130.126802](https://doi.org/10.1103/PhysRevLett.130.126802)

The interplay of magnetism and superconductivity is a central question in the study of strongly correlated electronic systems. In heavy fermion (HF) metals a particular advantage is the ability to tune the system to a quantum critical point (QCP), by pressure or some other tuning parameter, at which superconductivity can emerge. In YbRh₂Si₂ magnetic field provides a convenient tuning parameter, at ambient pressure, and without recourse to doping. However, superconductivity in YbRh₂Si₂ only appears at low mK temperatures, implying extremely low thermodynamic critical fields. The onset of strong magnetic screening and a heat capacity peak observed in the vicinity of 2 mK [1] have been interpreted in terms of a simultaneous superconducting and electronuclear magnetic phase transition. The experiment we report in this Letter focuses on a detailed and precise investigation of this transition, on establishing the magnetic ground state, and its evolution with magnetic field.

YbRh₂Si₂ has tetragonal symmetry and a theoretically predicted highly anisotropic, three-dimensional Fermi surface [2–6]. Antiferromagnetic (AFM) electronic order appears in zero applied field at $T_N = 70$ mK and features ultrasmall ordered moments, $\mu_e \approx 0.002\mu_B$ [7], which develop out of partially Kondo-screened Yb local moments $1.4\mu_B$ [8]. The nature of this order is not established, with an interesting possibility of the ordered moments aligned with the magnetically hard c axis [9]. Neutron scattering, above T_N , shows incommensurate AFM fluctuations which emerge from ferromagnetic (FM) fluctuations [10]. Static

magnetic susceptibility [11], NMR [12], and ESR [13–15] also provide evidence of FM fluctuations.

The observed suppression of T_N by magnetic field at ambient pressure on high quality samples first led to the proposal of a QCP, induced by an in-plane field of $B_c = 60$ mT, or 10 times larger field along the c axis [8], reflecting the highly anisotropic electronic magnetism. The nature of the putative QCP remains a matter of debate, including theories of local quantum criticality [16–19], see also [20–24], and theories invoking strong coupling of fermions and spin fluctuations into critical quasiparticles [25–27]. Negative chemical pressure, achieved by Ge doping, shifts the QCP to smaller fields [11,28], cobalt doping induces ferromagnetism [9,29].

Most recently, the report of superconductivity in YbRh₂Si₂ [1,30] led to the proposal that an important role is played by the coupling of electronic and nuclear magnetism. The strong hyperfine interaction and presence of active Yb nuclei distinguishes YbRh₂Si₂ from Ce-based HF systems, for which the nuclear moments are zero. Thus YbRh₂Si₂ provides a model system to investigate the influence of nuclear spins in a Kondo lattice exhibiting quantum criticality [31]. The ground state doublet of the Yb ion in the crystalline electric field (CEF) also distinguishes this system from systems with strong hyperfine interactions based on non-Kramers ions such as Pr and Ho [32]. The work reported here presents a first step to precisely thermodynamically characterize the interplay of electronic and nuclear magnetism in YbRh₂Si₂.

Our experimental setup exploits advances in current sensing noise thermometry [33]. This includes improvements in the speed of measurement achieved by a relatively high sensor resistance (a 0.2 Ω PtW wire), coupled with the ability to limit the heat leak into the noise thermometer to below 1 fW by appropriate shielding and filtering of the leads [34]. The single crystal of YbRh₂Si₂ from batch 63 129 with $RRR = 50$ [35] is thermalized via an aluminium wire, operating as a superconducting heat switch. A superconducting solenoid both provides the sample field and operates the heat switch. The heat capacity is determined by the adiabatic heat pulse method below 10 mT, the critical field of aluminium, and by the relaxation method above it.

The molar heat capacity in zero applied field, Fig. 1, shows the well-known Néel anomaly at $T_N = 70.5$ mK, and another sharp anomaly at $T_A = 1.5$ mK. The heat capacity measured around 1 mK exceeds the heavy-electron term $\gamma_S T$ by 3 orders of magnitude. We demonstrate that this large heat capacity originates from Yb nuclear degrees of freedom, however, the T_A anomaly reflects a cooperative transition involving both nuclei and electrons. On the other hand, above a few mK the nuclear heat capacity decreases as T^{-2} , while the electronic heat capacity increases linearly with temperature. As a result, above 20 mK the electronic part dominates (see Supplemental Material [36], Fig. S7), and thus at T_N the nuclear spin degrees of freedom play no role [37], contributing less than 1% to the heat capacity there. While the electronic moments form a regular lattice, only a minority of Yb sites carry a nuclear moment. Thus the low temperature heat capacity arises from the nuclei of ¹⁷¹Yb ($I = 1/2$) and ¹⁷³Yb ($I = 5/2$) isotopes with 0.1431 and 0.1613 natural abundances, respectively, distributed randomly across Yb sites. The nuclear spins are subject to an

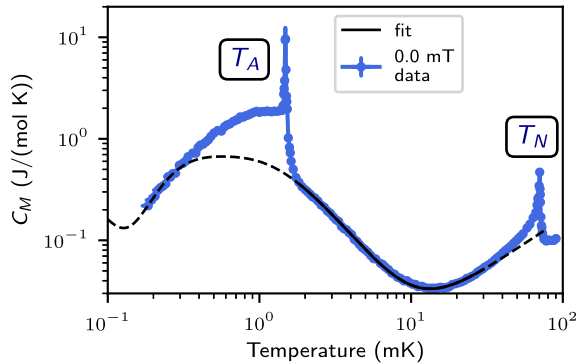


FIG. 1. Molar heat capacity in zero field exhibits two sharp anomalies at T_A and T_N that we identify with magnetic transitions. The data between 1.85 and 30 mK are fitted to the nuclear and heavy-electron heat capacity. The fit curve is plotted outside of the fitting interval as a dashed line. The small ordered electronic moments found above T_A [7] would significantly affect the nuclear heat capacity only below 0.2 mK.

effective hyperfine magnetic field $\mathbf{B}_{hf} = -A_{hf}\boldsymbol{\mu}_e$, produced by the ordered static part of Yb electronic moments $\boldsymbol{\mu}_e$. Here $A_{hf} = 102$ T/ μ_B is the hyperfine constant [38–40]. The “fast relaxation regime” realized in YbRh₂Si₂ [37,41–44], enables us to ignore the hyperfine field due to the fluctuating part of the electronic moments and treat $\boldsymbol{\mu}_e$ as a mean field. Additionally, the ¹⁷³Yb nuclei experience quadrupolar splitting in the crystalline electric field gradient, that points along the c axis.

We neglect interactions between nuclei and consider a single-spin Hamiltonian

$$\hat{H} = g\mu_N A_{hf} \hat{\mathbf{I}} \cdot \boldsymbol{\mu}_e + \frac{e^2 q Q}{4I(2I-1)} [3\hat{I}_z^2 - I(I+1)], \quad (1)$$

where g , μ_N , Q are the nuclear g factor, magneton, and quadrupole moment and eq represents the electric field gradient. In general the nuclear spin $\hat{\mathbf{I}}$ is not aligned with the c axis and Eq. (1) is diagonalized numerically, to calculate the partition function Z of the nuclear system, and hence thermodynamic quantities. These are summed over a random distribution of ¹⁷¹Yb and ¹⁷³Yb nuclei according to their natural abundance.

In the simplest case, the *Schottky model*, we assume uniform $\boldsymbol{\mu}_e$ on all Yb sites. Fitting the data above T_A unambiguously proves that the size of the static electronic moment in zero magnetic field is small, in agreement with measurements of muon spin resonance [7]. We put an upper bound $\boldsymbol{\mu}_e \ll 0.01\mu_B$ (in any direction) and directly determine the parameters of the quadrupole splitting. We find a positive electric field gradient $eq = (2.06 \pm 0.01) \times 10^{21}$ Vm⁻², less than half of the previously used estimates [37,42,45], and obtain the Sommerfeld coefficient $\gamma_S = (1.65 \pm 0.01)$ J/(mol K²), in good agreement with previous work [46].

Figure 2(a) shows the evolution of the T_A anomaly with magnetic field B_{ext} applied in the ab plane in the range 0.0–21.1 mT. The anomaly shifts to lower temperatures with increasing applied field, broadens, and possibly develops a structure (a split into a double peak is observed at 14.7 mT). Measurements in fields in the range 35.9–69.7 mT do not display any anomaly and their overall shape resembles a typical Schottky peak.

In all magnetic fields the data above T_A (or down to the lowest temperatures at $B_{\text{ext}} > 35.9$ mT, where the anomaly was not observed) are well described by the Schottky model, assuming paramagnetic polarization $\boldsymbol{\mu}_e \parallel \mathbf{B}_{\text{ext}}$, see Fig. 2(b). Fixing the quadrupolar parameters for ¹⁷³Yb at the zero field value, we find approximately linear growth of $\boldsymbol{\mu}_e$ with field up to $\approx 0.1\mu_B$ at $B_c = 60$ mT, with weaker increase at higher fields, Fig. 2(c), consistent with the magnetic susceptibility measurements [47–49]. More subtle effects, such as the temperature dependence of $\boldsymbol{\mu}_e$, may improve the agreement between the data and the model.

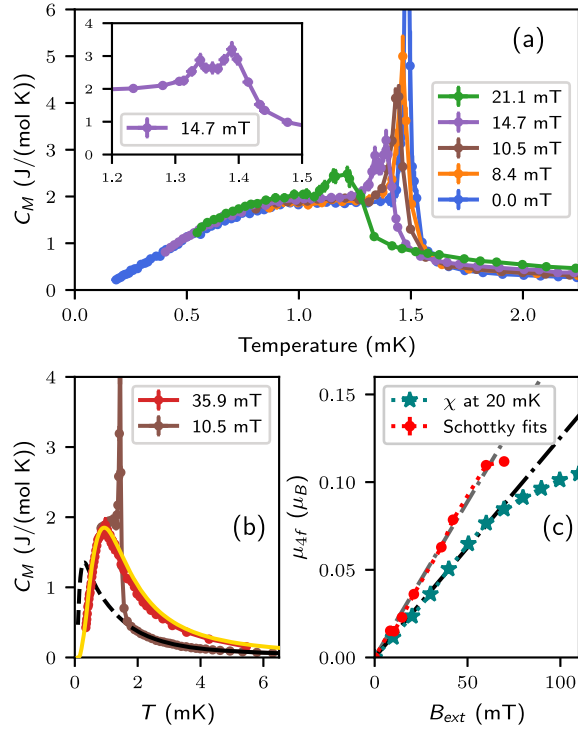


FIG. 2. Molar heat capacity in field applied in the ab plane. (a) Suppression of T_A anomaly with field. (b) Examples of fitting the Schottky model. Below 35.9 mT, where T_A is observed, only the data above this anomaly are fitted. (c) The static electronic moment of Yb determined from ac susceptibility χ [47] and from the Schottky model.

We now discuss the transition at T_A and the data down to the lowest temperatures. The entropy release below 10 mK matches well the full nuclear entropy of ^{171}Yb and ^{173}Yb , $S_{\text{Yb}} = 3.22 \text{ J}/(\text{mol K})$ in all magnetic fields, see Fig. S1 in Supplemental Material [36]. Under the conditions of our experiments the nuclear spins ^{29}Si and ^{103}Rh remain disordered and do not contribute to the heat capacity due to weak hyperfine constants for these elements.

Continuous warm-up measurements in zero magnetic field suggest, despite the sharpness of the heat capacity anomaly, that the phase transition is continuous, see Fig. S2 in Supplemental Material [36]. The majority of the Yb nuclear entropy is released below T_A , leaving only $0.06S_{\text{Yb}}$ for the transition region. This points to gradual ordering of Yb nuclear spins in the hyperfine field produced by the electronic moments and supports the picture of a nuclear-assisted electronic transition, developed later.

In zero magnetic field, the relatively slow decrease of the heat capacity with decreasing temperatures cannot be accounted for by the Schottky model with uniform μ_e , see Fig. 3. We therefore postulate a spatially modulated electronic order (SMO) state, with a sinusoidal distribution of the hyperfine field on the randomly distributed ^{171}Yb and ^{173}Yb nuclei (see inset in Fig. 3) produced by the electronic moments

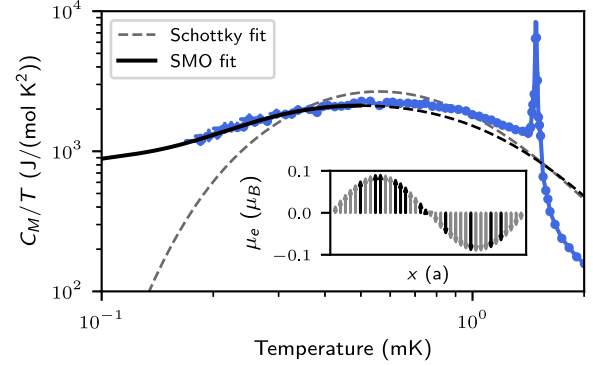


FIG. 3. Zero field C_M/T with the fit according to the SMO model below 0.5 mK; the “best fit” according to spatially homogeneous Schottky model clearly disagrees with the data. The inset: electronic moments in SMO, black arrows represent randomly distributed Yb sites with active nuclei.

$$\mu_e(\mathbf{r}) = \mu_A \hat{\mathbf{x}} \sin(\mathbf{r} \cdot \mathbf{q}), \quad (2)$$

where $\hat{\mathbf{x}}$ is a unit vector, that we assume to lie in the easy ab plane. The heat capacity derived from the SMO model is insensitive to \mathbf{q} , as long as it is small or incommensurate, leaving a single free parameter, the maximum value of the modulated electronic moment μ_A . The fit to the data below 0.5 mK yields $\mu_A = (0.093 \pm 0.001)\mu_B$. It is noteworthy that this is comparable with the size of the moment induced by the critical field of the T_N order, see Fig. 2(c). Nuclear magnetic resonance is an established tool to confirm the existence of a SMO, or a spin density wave (SDW), in the absence of direct evidence from neutron scattering. Here we demonstrate that the heat capacity of nuclei responding to electronic order is another powerful probe of SMO, albeit it does not allow us to determine \mathbf{q} in Eq. (2).

To account for the shape of the heat capacity anomaly, we make a simple ansatz for the temperature dependence of the order parameter

$$\mu_A(T) = \mu_A(T=0)|1 - T/T_A|^{\beta_c}. \quad (3)$$

For $\beta_c \approx 0.07$ the calculated heat capacity fits the zero-field data well across the whole temperature region, as shown in Fig. 4. The smallness of the critical exponent β_c and the resulting sharpness of the heat capacity peak demonstrate significant critical point fluctuations.

We now move to a simple mean-field model that captures the T_A transition. We argue that the mechanism behind this transition in the electronic magnetism is the hyperfine coupling of the static Yb electronic moments μ_e to the active Yb nuclei. The key is to recognize the fragility of the AFM order that emerges at T_N . The established dependence $\mu_e(B_{\text{ext}})$, Fig. 2(c), allows us to determine the magnetic Helmholtz free energy,

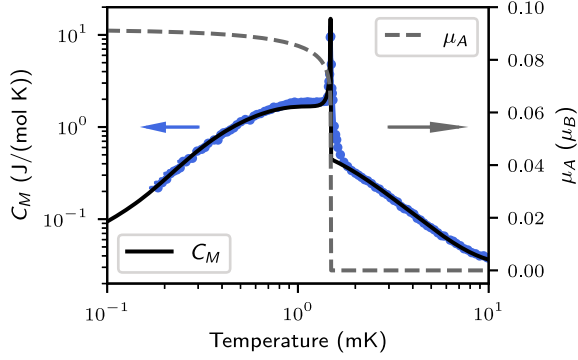


FIG. 4. Model of the zero-field heat capacity using a simple ansatz for the temperature dependence of the order parameter, Eq. (3).

$$F_e(\mu_e) = \int_0^{\mu_e} B d\mu'_e, \quad (4)$$

per Yb site. At $B_{\text{ext}} = B_c = 70$ mT, that suppresses the AFM order, we find $F_e(0.09\mu_B) \approx 2$ mK, much smaller than T_N . The consequence of this small scale is that the energy cost of an increase in electronic moment can be overcome by the reduction in the free energy of the nuclear spin system, polarized in the hyperfine field induced by these electronic moments.

To model the system through T_A in an in-plane field applied along a unit vector \hat{y} we consider electronic moments

$$\boldsymbol{\mu}_e(\mathbf{r}) = \mu_A \hat{\mathbf{x}} \sin(\mathbf{r} \cdot \mathbf{q}) + \mu_P \hat{\mathbf{y}}, \quad (5)$$

with mutually orthogonal modulated μ_A and paramagnetic μ_P components, both in the ab plane. The model does not consider the preexisting T_N order due to its small moments. We write the Gibbs free energy as

$$G(T, B_{\text{ext}}; \mu_A, \mu_P) = \sum_{\mathbf{r}} -k_B T \log Z(T, \boldsymbol{\mu}_e(\mathbf{r})) + N[\alpha\mu_A^2 + \beta\mu_P^2 + \gamma\mu_A^4 + \delta\mu_P^4 + \eta\mu_A^2\mu_P^2 - B_{\text{ext}}\mu_P], \quad (6)$$

where the sum is over the active Yb sites with different values of the static electronic moment and size of nuclear spin I and N is the total number of Yb sites in the system. At each site the nuclear partition function Z is evaluated numerically from the Hamiltonian in Eq. (1). The phenomenological energy of the electronic order is expanded up to the fourth order in μ_A and μ_P , retaining only the terms allowed by symmetry. The electronic order parameters $\mu_A(T, B_{\text{ext}})$ and $\mu_P(T, B_{\text{ext}})$ are found by minimising G , then the entropy and heat capacity are evaluated (see Supplemental Material [36]).

The model successfully captures most features of the experimental data, see Fig. 5. Here $\beta = 1/(2\chi) \approx 0.4$ T/ μ_B

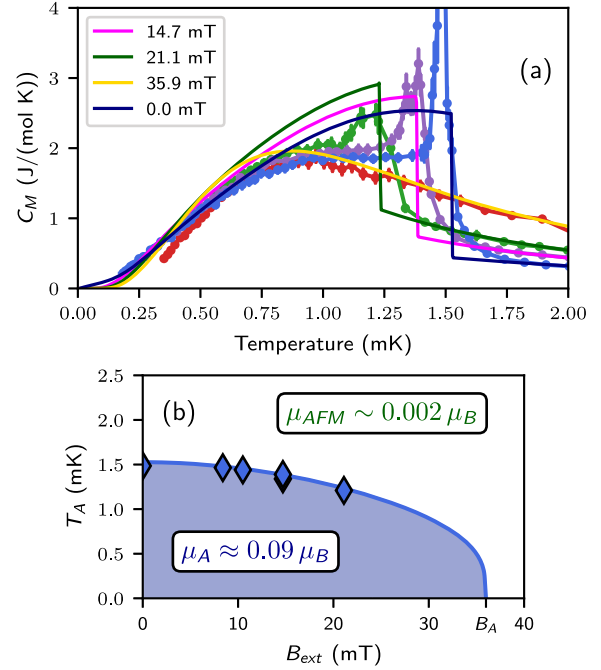


FIG. 5. Comparison of the experimental data to the phenomenological mean-field model based on Eq. (6). (a) Heat capacity. The sharpness of the anomaly is the only major feature not captured by the model. (b) Phase diagram of SMO in YbRh_2Si_2 . Diamonds and straight line represent the experimental data and model, respectively.

and $\delta = 0$ are fixed from the susceptibility measured at $T > T_A$ [47]; $\alpha \approx 0.026$ T/ μ_B is determined from T_A at zero field; the nonessential 4th order terms $\gamma \approx 0.2$ T/ μ_B^3 and $\eta \approx 4$ T/ μ_B^3 improve the agreement with the measured temperature dependence of the heat capacity below T_A and the suppression of T_A with field.

At zero magnetic field the SMO is established via a second-order phase transition. In-plane field additionally induces the paramagnetic component μ_P , similar to that shown in Fig. 2(c), and gradually suppresses T_A and μ_A , but the transition remains second order up to the ultimate suppression of SMO at $B_A = 36$ mT. Both T_A and B_A are sensitive to the Yb isotopic composition. The key features of this numerical model are illustrated by a simple analytic $I = 1/2$ model in the Supplemental Material [36].

We conclude by discussing the insight provided by these heat capacity measurements on superconductivity in YbRh_2Si_2 [1,30,49–52]. The heat capacity signature at T_A is well aligned in temperature with an abrupt change in the shielding factor [1,49,51] and sample electrical impedance [52]. According to Ref. [1], the superconducting transition occurs in the vicinity of T_A , however, both the magnetic shielding [1,51] and electrical transport [30,52] exhibit sharp onset of superconductivity around 10 mK. At T_A the nuclear heat capacity dominates the heavy-electron term by at least 3 orders of magnitude. Therefore any anomaly in the electronic heat capacity associated with a

BCS-like superconducting transition at that temperature is undetectable in these measurements. On the other hand at 6–12 mK our data would reveal such a signature against the nuclear quadrupole background (see Supplemental Material [36], Fig. S9). Its absence points towards inhomogeneous superconductivity.

References [1,50] postulated competition between electronic magnetism and the superconductivity, and proposed that the latter is only established after the former is weakened at T_A . By contrast we find that below T_A , where the superconductivity is more robust, the electronic magnetism is simultaneously strengthened. Whether the AFM order established at T_N is suppressed below T_A remains an open question. The two magnetic orders may coexist and even share the same \mathbf{q} (more in Supplemental Material [36]).

The observation of superconductivity both above and below T_A opens an intriguing possibility of different superconducting order parameters in these regimes. The superconductivity and SMO may be intertwined, forming a pair density wave [53,54] below T_A .

Our heat capacity method should be applied to the investigation of isotopically enriched samples. This includes potential nuclear spin ordering in $^{171}\text{YbRh}_2\text{Si}_2$ and $^{173}\text{YbRh}_2\text{Si}_2$, as well as heavy-fermion quantum criticality in $^{174}\text{YbRh}_2\text{Si}_2$, in the absence of nuclear magnetism.

We demonstrated how strong hyperfine interactions can give rise to a nuclear-assisted transition in the electronic magnetism at a temperature below the onset of superconductivity. This offers a fresh opportunity to further the understanding of the interplay between magnetism and superconductivity, accessible by new experimental techniques which extend studies of strongly correlated electron systems into the microkelvin regime.

This work was supported by European Union's Horizon 2020 Research and Innovation programme under Grant Agreement No. 824109 (European Microkelvin Platform) and the Deutsche Forschungsgemeinschaft (DFG, German Research Foundation) through Grants No. BR 4110/1-1, No. KR3831/4-1, via the TRR 288 (422213477, project A03), and via a Leverhulme Trust Research grant. We would like to thank Piers Coleman and Séamus Davis for helpful discussions.

*jan.knapp@rhul.ac.uk

[†]l.v.levitin@rhul.ac.uk

[‡]j.saunders@rhul.ac.uk

- [1] E. Schuberth, M. Tippmann, L. Steinke, S. Lausberg, A. Steppke, M. Brando, C. Krellner, C. Geibel, R. Yu, Q. Si, and F. Steglich, Emergence of superconductivity in the canonical heavy-electron metal YbRh_2Si_2 , *Science* **351**, 485 (2016).
- [2] S. Friedemann, S. Wirth, N. Oeschler, C. Krellner, C. Geibel, F. Steglich, S. MaQuilon, Z. Fisk, S. Paschen, and G. Zwicknagl, Hall effect measurements and electronic

structure calculations on YbRh_2Si_2 and its reference compounds LuRh_2Si_2 and YbIr_2Si_2 , *Phys. Rev. B* **82**, 035103 (2010).

- [3] K. Kummer, S. Patil, A. Chikina, M. Güttler, M. Höppner, A. Generalov, S. Danzenbächer, S. Seiro, A. Hannaske, C. Krellner, Y. Kucherenko, M. Shi, M. Radovic, E. Rienks, G. Zwicknagl, K. Matho, J. W. Allen, C. Laubschat, C. Geibel, and D. V. Vyalikh, Temperature-Independent Fermi Surface in the Kondo Lattice YbRh_2Si_2 , *Phys. Rev. X* **5**, 011028 (2015).
- [4] G. Zwicknagl, The utility of band theory in strongly correlated electron systems, *Rep. Prog. Phys.* **79**, 124501 (2016).
- [5] Y. Li, Q. Wang, Y. Xu, W. Xie, and Y.F. Yang, Nearly degenerate $p_x + ip_y$ and $d_{x^2-y^2}$ pairing symmetry in the heavy fermion superconductor YbRh_2Si_2 , *Phys. Rev. B* **100**, 085132 (2019).
- [6] M. Güttler, K. Kummer, K. Kliemt, C. Krellner, S. Seiro, C. Geibel, C. Laubschat, Y. Kubo, Y. Sakurai, D. V. Vyalikh, and A. Koizumi, Visualizing the Kondo lattice crossover in YbRh_2Si_2 with Compton scattering, *Phys. Rev. B* **103**, 115126 (2021).
- [7] K. Ishida, D. E. MacLaughlin, B. L. Young, K. Okamoto, Y. Kawasaki, Y. Kitaoka, G. J. Nieuwenhuys, R. H. Heffner, O. O. Bernal, W. Higemoto, A. Koda, R. Kadono, O. Trovarelli, C. Geibel, and F. Steglich, Low-temperature magnetic order and spin dynamics in YbRh_2Si_2 , *Phys. Rev. B* **68**, 184401 (2003).
- [8] P. Gegenwart, J. Custers, C. Geibel, K. Neumaier, T. Tayama, K. Tenya, O. Trovarelli, and F. Steglich, Magnetic-Field Induced Quantum Critical Point in YbRh_2Si_2 , *Phys. Rev. Lett.* **89**, 056402 (2002).
- [9] S. Hamann, J. Zhang, D. Jang, A. Hannaske, L. Steinke, S. Lausberg, L. Pedrero, C. Klingner, M. Baenitz, F. Steglich, C. Krellner, C. Geibel, and M. Brando, Evolution from Ferromagnetism to Antiferromagnetism in $\text{Yb}(\text{Rh}_{1-x}\text{Co}_x)\text{Si}_2$, *Phys. Rev. Lett.* **122**, 077202 (2019).
- [10] C. Stock, C. Broholm, F. Demmel, J. Van Duijn, J. W. Taylor, H. J. Kang, R. Hu, and C. Petrovic, From Incommensurate Correlations to Mesoscopic Spin Resonance in YbRh_2Si_2 , *Phys. Rev. Lett.* **109**, 127201 (2012).
- [11] P. Gegenwart, J. Custers, Y. Tokiwa, C. Geibel, and F. Steglich, Ferromagnetic Quantum Critical Fluctuations in $\text{YbRh}_2(\text{Si}_{0.95}\text{Ge}_{0.05})_2$, *Phys. Rev. Lett.* **94**, 076402 (2005).
- [12] K. Ishida, K. Okamoto, Y. Kawasaki, Y. Kitaoka, O. Trovarelli, C. Geibel, and F. Steglich, YbRh_2Si_2 : Spin Fluctuations in the Vicinity of a Quantum Critical Point at Low Magnetic Field, *Phys. Rev. Lett.* **89**, 107202 (2002).
- [13] J. Sichelschmidt, V. A. Ivashin, J. Ferstl, C. Geibel, and F. Steglich, Low Temperature Electron Spin Resonance of the Kondo ion in a Heavy Fermion Metal: YbRh_2Si_2 , *Phys. Rev. Lett.* **91**, 156401 (2003).
- [14] E. Abrahams and P. Wölfle, Electron spin resonance in Kondo systems, *Phys. Rev. B* **78**, 104423 (2008).
- [15] P. Wölfle and E. Abrahams, Phenomenology of ESR in heavy-fermion systems: Fermi-liquid and non-Fermi-liquid regimes, *Phys. Rev. B* **80**, 235112 (2009).
- [16] Q. Si, S. Rabello, K. Ingersent, and J. L. Smith, Locally critical quantum phase transitions in strongly correlated metals, *Nature (London)* **413**, 804 (2001).

- [17] P. Coleman and A. J. Schofield, Quantum criticality, *Nature (London)* **433**, 226 (2005).
- [18] Q. Si and F. Steglich, Heavy Fermions and quantum phase transitions, *Science* **329**, 1161 (2010).
- [19] F. Steglich, Heavy fermions: Superconductivity and its relationship to quantum criticality, *Philos. Mag.* **94**, 3259 (2014).
- [20] M. H. Schubert, Y. Tokiwa, S. H. Hübner, M. Mchawat, E. Blumenröther, H. S. Jeevan, and P. Gegenwart, Tuning low-energy scales in YbRh_2Si_2 by non-isoelectronic substitution and pressure, *Phys. Rev. Res.* **1**, 032004(R) (2019).
- [21] P. Gegenwart, T. Westerkamp, C. Krellner, Y. Tokiwa, S. Paschen, C. Geibel, F. Steglich, E. Abrahams, and Q. Si, Multiple energy scales at a quantum critical point, *Science* **315**, 969 (2007).
- [22] P. Gegenwart, Q. Si, and F. Steglich, Quantum criticality in heavy-fermion metals, *Nat. Phys.* **4**, 186 (2008).
- [23] S. Paschen and Q. Si, Quantum phases driven by strong correlations, *Nat. Rev. Phys.* **3**, 9 (2020).
- [24] E. Schuberth, S. Wirth, and F. Steglich, Nuclear-order-induced quantum criticality and Heavy-Fermion superconductivity at ultra-low temperatures in YbRh_2Si_2 , *Front. Electron. Mater.* **2**, 869495 (2022).
- [25] E. Abrahams and P. Wölfle, Critical quasiparticle theory applied to heavy fermion metals near an antiferromagnetic quantum phase transition, *Proc. Natl. Acad. Sci. U.S.A.* **109**, 3238 (2012).
- [26] E. Abrahams, J. Schmalian, and P. Wölfle, Strong-coupling theory of heavy-fermion criticality, *Phys. Rev. B* **90**, 045105 (2014).
- [27] P. Wölfle and E. Abrahams, Spin-flip scattering of critical quasiparticles and the phase diagram of YbRh_2Si_2 , *Phys. Rev. B* **92**, 155111 (2015).
- [28] J. Custers, P. Gegenwart, H. Wilhelm, K. Neumaier, Y. Tokiwa, O. Trovarelli, C. Geibel, F. Steglich, C. Pépin, and P. Coleman, The break-up of heavy electrons at a quantum critical point, *Nature (London)* **424**, 524 (2003).
- [29] S. Lausberg, A. Hannaske, A. Steppke, L. Steinke, T. Gruner, L. Pedrero, C. Krellner, C. Klingner, M. Brando, C. Geibel, and F. Steglich, Doped YbRh_2Si_2 : Not Only Ferromagnetic Correlations But Ferromagnetic Order, *Phys. Rev. Lett.* **110**, 256402 (2013).
- [30] D. Nguyen, A. Sidorenko, M. Taupin, G. Knebel, G. Lapertot, E. Schuberth, and S. Paschen, Superconductivity in an extreme strange metal, *Nat. Commun.* **12**, 4341 (2021).
- [31] H. Eisenlohr and M. Vojta, Limits to magnetic quantum criticality from nuclear spins, *Phys. Rev. B* **103**, 064405 (2021).
- [32] M. Libersky, R. D. McKenzie, D. M. Silevitch, P. C. E. Stamp, and T. F. Rosenbaum, Direct Observation of Collective Electronuclear Modes About a Quantum Critical Point, *Phys. Rev. Lett.* **127**, 207202 (2021).
- [33] A. Casey, F. Arnold, L. V. Levitin, C. P. Lusher, J. Nyéki, J. Saunders, A. Shibahara, H. van der Vliet, B. Yager, D. Drung, T. Schurig, G. Batey, M. N. Cuthbert, and A. J. Matthews, Current sensing noise thermometry: A fast practical solution to low temperature measurement, *J. Low Temp. Phys.* **175**, 764 (2014).
- [34] L. Levitin, H. van der Vliet, T. Theisen, S. Dimitriadis, M. Lucas, A. Corcoles, J. Nyéki, A. Casey, G. Creeth, I. Farrer, D. Ritchie, J. Nicholls, and J. Saunders, Cooling low-dimensional electron systems into the microkelvin regime, *Nat. Commun.* **13**, 1 (2022).
- [35] C. Krellner, S. Taube, T. Westerkamp, Z. Hossain, and C. Geibel, Single-crystal growth of YbRh_2Si_2 and YbIr_2Si_2 , *Philos. Mag.* **92**, 2508 (2012).
- [36] See Supplemental Material at <http://link.aps.org/supplemental/10.1103/PhysRevLett.130.126802> for entropy analysis, additional discussion of the T_A transition, further analysis of the zero-field heat capacity, details of the mean-field model.
- [37] G. Knebel, R. Boursier, E. Hassinger, G. Lapertot, P. G. Niklowitz, A. Pourret, B. Salce, J. P. Sanchez, I. Sheikin, P. Bonville, H. Harima, and J. Flouquet, Localization of 4f state in YbRh_2Si_2 under magnetic field and high pressure: Comparison with CeRh_2Si_2 , *J. Phys. Soc. Jpn.* **75**, 114709 (2006).
- [38] J. Kondo, Internal magnetic field in rare earth metals, *J. Phys. Soc. Jpn.* **16**, 1690 (1961).
- [39] P. Bonville, P. Imbert, G. Jéhanno, F. Gonzalez-Jimenez, and F. Hartmann-Boutron, Emission Mössbauer spectroscopy and relaxation measurements in hyperfine levels out of thermal equilibrium: Very-low-temperature experiments on the Kondo alloy Au^{170}Yb , *Phys. Rev. B* **30**, 3672 (1984).
- [40] P. Bonville, J. A. Hodges, P. Imbert, G. Jéhanno, D. Jaccard, and J. Sierro, Magnetic ordering and paramagnetic relaxation of Yb^{3+} in YbNi_2Si_2 , *J. Magn. Magn. Mater.* **97**, 178 (1991).
- [41] I. Nowik and S. Ofer, Mössbauer studies of ^{170}Yb in several paramagnetic salts, *J. Phys. Chem. Solids* **29**, 2117 (1968).
- [42] J. Plessel, M. M. Abd-Elmeguid, J. P. Sanchez, G. Knebel, C. Geibel, O. Trovarelli, and F. Steglich, Unusual behavior of the low-moment magnetic ground state of YbRh_2Si_2 under high pressure, *Phys. Rev. B* **67**, 180403(R) (2003).
- [43] J. Flouquet and W. D. Brewer, Hyperfine interaction studies of local moments in metals, *Phys. Scr.* **11**, 199 (1975).
- [44] J. Flouquet, Kondo coupling, hyperfine and exchange interactions, *J. Phys. Colloq.* **39**, C6 (1978).
- [45] A. Steppke, M. Brando, N. Oeschler, C. Krellner, C. Geibel, and F. Steglich, Nuclear contribution to the specific heat of $\text{Yb}(\text{Rh}_{0.93}\text{Co}_{0.07})_2\text{Si}_2$, *Phys. Status Solidi (b)* **247**, 737 (2010).
- [46] C. Krellner, S. Hartmann, A. Pikul, N. Oeschler, J. G. Donath, C. Geibel, F. Steglich, and J. Wosnitzer, Violation of Critical Universality at the Antiferromagnetic Phase Transition of YbRh_2Si_2 , *Phys. Rev. Lett.* **102**, 196402 (2009).
- [47] M. Brando, L. Pedrero, T. Westerkamp, C. Krellner, P. Gegenwart, C. Geibel, and F. Steglich, Magnetization study of the energy scales in YbRh_2Si_2 under chemical pressure, *Phys. Status Solidi (b)* **250**, 485 (2013).
- [48] S. Friedemann, T. Westerkamp, M. Brando, N. Oeschler, S. Wirth, P. Gegenwart, C. Krellner, C. Geibel, and F. Steglich, Detaching the antiferromagnetic quantum critical point from the Fermi-surface reconstruction in YbRh_2Si_2 , *Nat. Phys.* **5**, 465 (2009).
- [49] L. Steinke, E. Schuberth, S. Lausberg, M. Tippmann, A. Steppke, C. Krellner, C. Geibel, F. Steglich, and M. Brando, Ultra-low temperature ac susceptibility of the

- heavy-fermion superconductor YbRh_2Si_2 , *J. Phys. Conf. Ser.* **807**, 052007 (2017).
- [50] M. Smidman *et al.*, Interplay between unconventional superconductivity and heavy-fermion quantum criticality: CeCu_2Si_2 versus YbRh_2Si_2 , *Philos. Mag.* **98**, 2930 (2018).
- [51] P. Knappová *et al.*, Study of superconducting regimes in YbRh_2Si_2 using dc-magnetisation and susceptibility (to be published).
- [52] L. V. Levitin *et al.*, Multiple superconducting transport regimes in heavy fermion metal YbRh_2Si_2 (to be published).
- [53] X. Liu, Y. Chong, R. Sharma, and S. Davis, Discovery of a Cooper-pair density wave state in a transition-metal dichalcogenide, *Science* **372**, 1447 (2021).
- [54] E. Fradkin, S. A. Kivelson, and J. M. Tranquada, Colloquium: Theory of intertwined orders in high temperature superconductors, *Rev. Mod. Phys.* **87**, 457 (2015).

Correction: Support information in the Acknowledgments was incomplete and has been fixed.